taken at three different points along the channel show that the separation resolution is improved as DNA bands migrate along the channel (*21*).

The separation capability of the device was retained even at higher average electric fields. Separation of peaks could still be observed even at electric fields as high as 128 V/cm (*26*). This value is much higher than typical running electric fields in PFGE (1 to 10 V/cm). The use of such a high electric field, as well as the use of a dc field (no pulsing as in PFGE), greatly enhances the speed of the separation in our device because the channel structure ensures that DNA molecules relax to equilibrium size before they meet another constriction. In PFGE, the relaxation of DNA is achieved by pulsing the electric field.

The above results demonstrate the potential of this device as an efficient separation system for long DNA molecules. In addition to more efficient separation, this nanofluidic channel device can separate and analyze small amounts of DNA. The recovery of DNA molecules after separation is straightforward. The device can be modified to separate smaller or larger DNA molecules as well as various proteins and other polymers. The separation mechanism we have used will be valid for molecules with a radius of gyration larger than the gap width. Several separation channels, optimized for different length ranges of DNA, can be integrated in parallel for single-run sorting and analysis of various DNA samples. The fabrication method does not require high-resolution lithography techniques. There should be no serious technical barrier in making much thicker or thinner constrictions required for application of the device to a wider range of DNA sizes (*27*). The simplicity of the device will make theoretical modeling easier for further improvement, ultimately enabling its mass production and integration into a future μ-TAS.

References and Notes

1. J. Sudor and M. V. Novotny, *Anal. Chem.* **66**, 2446 (1994).
2. Y. Kim and M. D. Morris, *Anal. Chem.* **66**, 3081 (1994).
3. _____, *Anal. Chem.* **67**, 784 (1995).
4. In addition, concerns were raised [L. Mitnik, C. Heller, J. Prost, J. L. Viovy, *Science* **267**, 219 (1995)] over DNA aggregation in PFCGE caused by an electrohydrodynamic instability that sometimes results in spurious and irreproducible peaks.
5. D. T. Burke, M. A. Burns, C. Mastrangelo, *Genome Res.* **7**, 189 (1997).
6. M. A. Burns *et al.*, *Science* **282**, 484 (1998).
7. W. D. Volkmuth and R. H. Austin, *Nature* **358**, 600 (1992).
8. W. D. Volkmuth *et al.*, *Phys. Rev. Lett.* **72**, 2117 (1994).
9. T. A. J. Duke, R. H. Austin, E. C. Cox, S. S. Chan, *Electrophoresis* **17**, 1075 (1996).
10. S. W. Turner, A. M. Perez, A. Lopez, H. G. Craighead, *J. Vac. Sci. Technol. B* **16**, 3835 (1998).
11. H. P. Chou, C. Spence, A. Scherer, S. Quake, *Proc. Natl. Acad. Sci. U.S.A.* **96**, 11 (1999).
12. C. F. Chou *et al.*, *Proc. Natl. Acad. Sci. U.S.A.* **96**, 13762 (1999).
13. J. Han and H. G. Craighead, *J. Vac. Sci. Technol. A* **17**, 2142 (1999).
14. J. Han, S. W. Turner, H. G. Craighead, *Phys. Rev. Lett.* **83**, 1688 (1999).
15. First, a thin channel was etched into the substrate, then an additional lithography process defined the thick regions in the channel. Fabrication does not require high-resolution lithography techniques, as the fine dimension is controlled by an etch depth. Loading holes were made by potassium hydroxide (KOH) wet etching, and the device was sealed by anodic bonding to a thin glass plate. The same device could also be made using more sophisticated methods (*10*). Small reservoirs were made at both ends of the channel and the device was filled with buffer solution.
16. DNA used in this work was purchased from Sigma, New England Biolabs, and Gibco BRL. DNA was labeled with YOYO-1 dye (Molecular Probes) at a dye/base pair ratio of 1:10. As a buffer solution, tris-borate-EDTA (TBE) buffer at 5× concentration was used. This high concentration of the buffer effectively quenched the electro-osmosis of the channel without using any other surface modification agents.
17. An inverted microscope (Olympus IX-70) with fluorescence filter set (XF-100, Omega Optical Inc.) was used to detect the fluorescence signal from dyed DNA. Microscope images were recorded by an ICCD camera (ICCD-350F, Videoscope Intl.) into video format.
18. To get an electrophoregram, we electronically defined a region of interest (typically 50 to 150 μm wide) at the end of the channel and summed the fluorescence signal from that area every 0.5 to 1 s. This analysis was done with a video image processor (DVP-32, Instrutech Co.).
19. J. C. Giddings, *Unified Separation Science* (Wiley-Interscience, New York, 1991), pp. 96–105.
20. The main source of dispersion is not the diffusion of the molecules, but the statistical variation of the trapping time. The escape of DNA from a trap follows the same statistics as a radioactive decay. The standard deviation of trapping lifetime also increases with the average trapping lifetime. This increases the band dispersion at low fields. Diffusion of DNA in the channel is virtually blocked by the existence of the thin regions. In previous single-molecule experiments (*13*), we could not observe any diffusion across the thin region barrier in the absence of an applied field.
21. Additional data are available at www.sciencemag.org/feature/data/1046112.shl.
22. The DNA ladder samples used in the experiment were the Mono Cut Mix (New England Biolabs) and 5-kb ladder (Gibco BRL). The Mono Cut Mix sample contains DNA molecules ranging from 1.5 to 48 kbp; the 5-kb ladder contains 5-kbp DNA molecules and multiples up to 40 kbp. The concentration (6.38 μg/ml) and the dye/base pair ratio (1:10) of both DNA solutions were the same.
23. In other data with higher ICCD gain settings, the 1.5-kbp peak was identified as a tiny peak in the electrophoregram. In such a case, however, the ICCD was saturated by brighter peaks, yielding a poor electrophoregram in the 20- to 48-kbp region. This is due to the limited dynamic range of the ICCD camera. Other detectors would be used in a real separation device as opposed to a research system.
24. An increase in the thin region depth may bring about better separation with even longer DNA molecules. The thin region depth corresponds to the average pore size of a gel, which in a conventional gel can be controlled only by changing the concentration of the gel. However, in our system, one can reliably define the thin region depth to a high accuracy in the fabrication process.
25. R. S. Madabhushi *et al.*, *Electrophoresis* **18**, 104 (1997).
26. Smaller DNA can be separated at a higher electric field because of its shorter relaxation time.
27. The fabrication method used here is expected to work for channels less than 50 nm thick.

28. We thank S. W. Turner, R. H. Austin, and E. Cox for their helpful suggestions, and R. Wu and S. Dai for helping in slab gel PFGE work. Supported by NIH grant HG01597.

8 October 1999; accepted 30 March 2000

Structure of the Hydrated α-Al_2O_3 (0001) Surface

Peter J. Eng,[1]* Thomas P. Trainor,[2] Gordon E. Brown Jr.[2,3] Glenn A. Waychunas,[4] Matthew Newville,[1] Stephen R. Sutton,[1] Mark L. Rivers[1,5]

The physical and chemical properties of the hydrated α-Al_2O_3 (0001) surface are important for understanding the reactivity of natural and synthetic aluminum-containing oxides. The structure of this surface was determined in the presence of water vapor at 300 kelvin by crystal truncation rod diffraction at a third-generation synchrotron x-ray source. The fully hydrated surface is oxygen terminated, with a 53% contracted double Al layer directly below. The structure is an intermediate between α-Al_2O_3 and γ-$Al(OH)_3$, a fully hydroxylated form of alumina. A semiordered oxygen layer about 2.3 angstroms above the terminal oxygen layer is interpreted as adsorbed water. The clean α-Al_2O_3 (0001) surface, in contrast, is Al terminated and significantly relaxed relative to the bulk structure. These differences explain the different reactivities of the clean and hydroxylated surfaces.

The interaction of water with solid surfaces plays an important role in many natural and technological processes, from mineral dissolution and adsorption/desorption reactions and the reaction of water with sulfate aerosol particles in the troposphere to corrosion of metals and the cleaning of semiconductor surfaces (*1*). Many previous studies of solid-water interfacial reactions have assumed that the solid surface is a perfect termination of the bulk structure, unmodified by hydration, but this assumption is almost certainly not true, even after short exposures to a humid atmosphere (*1*–*4*). This is important because the reactivity of metal oxide surfaces is strongly influenced by the degree of surface hydroxylation.

The hydrated α-Al_2O_3 (0001) surface is an important model system for understanding the reactivity of naturally abundant phases of Al-containing (hydr)oxides such as gibbsite or hydrous aluminosilicate clays due to similarity in coordination chemistry of Al in these phases. Particular attention has been paid to the reaction of water with the α-Al_2O_3 (0001) surface because of its importance as a model for hydration of environmental substrates (*5*) and as a reactive substrate in the atmosphere produced by the exhaust gases of solid rocket motors (*6, 7*). Alumina is also used extensively as a substrate for heterogeneous catalysis and the growth of thin metal and semiconductor films for various applications and as an adsorbent in wastewater treatment. Because of these and other applications, the structure of the α-Al_2O_3 (0001) surface has been the subject of much recent theoretical (*8–14*) and experimental work (*15–17*). In general, knowledge about the structure of hydrated metal oxide surfaces is required for testing models of the structure, reactivity, and charging behavior of metal-(hydr)oxide surfaces (*18, 19*).

We have used the recently developed technique of crystal truncation rod (CTR) diffraction (*20*), at a high-brilliance third-generation, synchrotron x-ray source to determine the structure of the hydrated α-Al_2O_3 (0001) surface under ambient conditions. Unlike the vacuum-prepared clean surface for which Al-terminated (*16, 17*) or mixed Al/O-terminated surfaces (*15*) have been reported, the hydrated surface is oxygen terminated, with a 53% contracted double aluminum layer directly below. A laterally disordered oxygen layer about 2.3 Å above the terminal oxygen layer is interpreted to be adsorbed water.

A highly polished single crystal (0001) wafer of α-Al_2O_3 was used. After a clean-and-wash procedure (*21*), the sample was characterized by x-ray photoelectron spectroscopy (XPS), which showed that the surface is composed of Al, O, and adventitious C. In previous photoemission studies of the hydroxylation of the clean alumina (0001) surface, a water vapor pressure of about 1 torr was sufficient to fully hydroxylate the surface (*22*). Therefore, the surface is expected to be fully hydroxylated after the wash procedure.

Measurements were performed at the Advanced Photon Source (APS) Argonne, Illinois, on the GeoSoilEnviroCARS beamline 13-ID. X-rays from the first harmonic of APS undulator "A" were monochromatized to 10 keV by using a Si(220) monochromator and focused to a spot size of 100 × 100 μm. Diffraction data were collected on the sample under ambient conditions (relative humidity >40%). A total of 882 structure factors were determined by integrating rocking scans through the crystal truncation rods (*23*). After symmetry equivalents were averaged, the final data set consisted of 525 unique data points from 10 crystal truncation rods (Fig. 1A).

Nonlinear least-squares fits of the full data set to a model consisting of a fixed bulk structure (*24*) of α-Al_2O_3 and an adjustable surface region were determined. Three chemically distinct (0001) terminations are possible for α-Al_2O_3: a double Al termination, a single Al termination, and an oxygen termination (*25*). Each of these terminations was tested in the fitting procedure, and the oxygen-terminated surface was found to give the best fit to the data. The calculated CTRs for the unrelaxed oxygen-terminated surface (Fig. 1A, dotted lines) show large misfits in the (10L) and (20L) rods. Allowing the surface atoms to relax from their bulk lattice positions resulted in a χ^2 value of 1.58 with the fit shown as dashed lines in Fig. 1A.

Allowing the oxygen-terminated bulk model to relax gives a good overall fit of the CTR data. However, there is a systematic deviation at low L for rods with nonzero H and K as well as poor agreement with the broad feature centered at L = 4 on the (00L) rod (Fig. 1A). These mismatches suggest that an additional component with a large disorder term is required. To address this, we added an oxygen overlayer with its own disorder term, which was intended to simulate a partly ordered physisorbed (hydrogen-bonded) water layer. This model is consistent with the re-

[1]Consortium for Advanced Radiation Sources, The University of Chicago, Chicago, IL 60637, USA. [2]Department of Geological and Environmental Sciences, Stanford University, Stanford, CA 94305–2115, USA. [3]Stanford Synchrotron Radiation Laboratory, Stanford, CA 94309, USA. [4]Earth Sciences Division, Lawrence Berkeley National Laboratory, Berkeley, CA 94720, USA. [5]Department of Geophysical Sciences, The University of Chicago, Chicago, IL 60637, USA.

*To whom correspondence should be addressed. E-mail: eng@cars.uchicago.edu

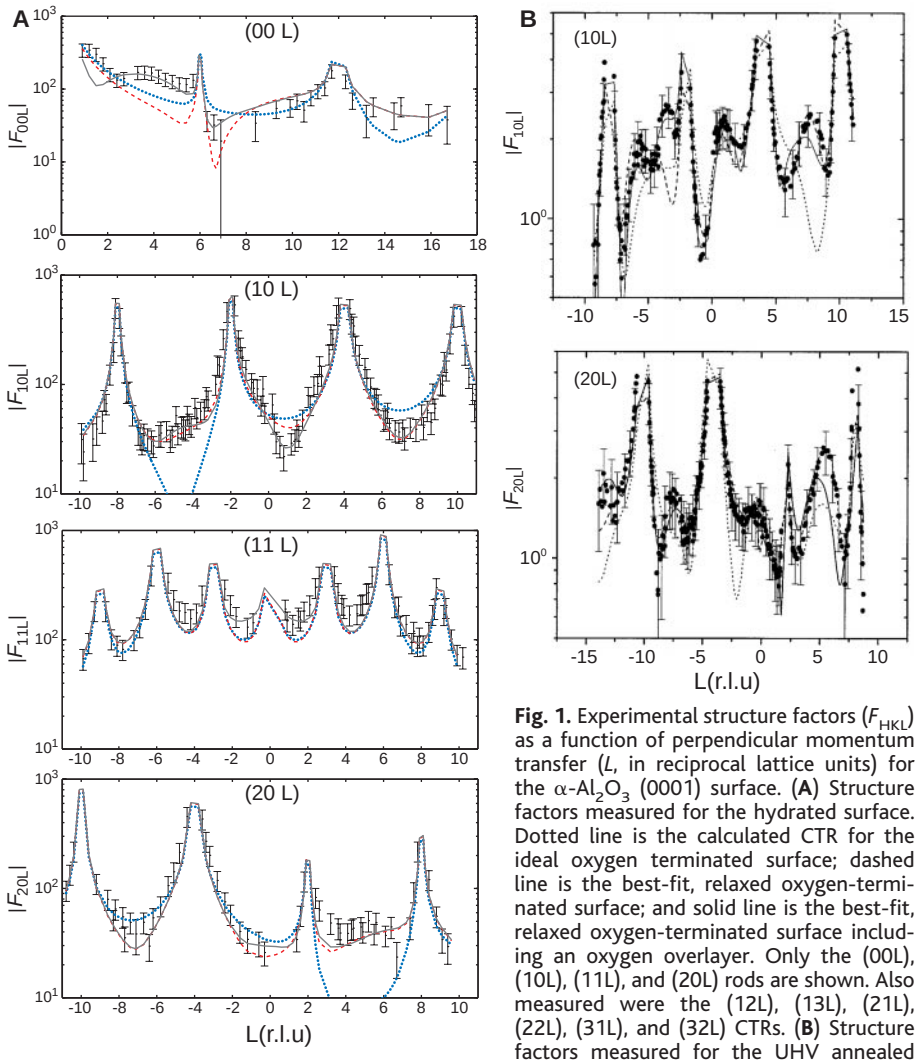

Fig. 1. Experimental structure factors (F_{HKL}) as a function of perpendicular momentum transfer (*L*, in reciprocal lattice units) for the α-Al_2O_3 (0001) surface. (**A**) Structure factors measured for the hydrated surface. Dotted line is the calculated CTR for the ideal oxygen terminated surface; dashed line is the best-fit, relaxed oxygen-terminated surface; and solid line is the best-fit, relaxed oxygen-terminated surface including an oxygen overlayer. Only the (00L), (10L), (11L), and (20L) rods are shown. Also measured were the (12L), (13L), (21L), (22L), (31L), and (32L) CTRs. (**B**) Structure factors measured for the UHV annealed clean surface by Guenard *et al*. (*17*). Solid line is the best-fit, single Al-terminated surface; dashed line is the best-fit, double Al terminated surface; and dotted line is the best-fit, oxygen-terminated surface. Differences in the structure of the measured CTRs shows the sensitivity of the technique to various terminations.

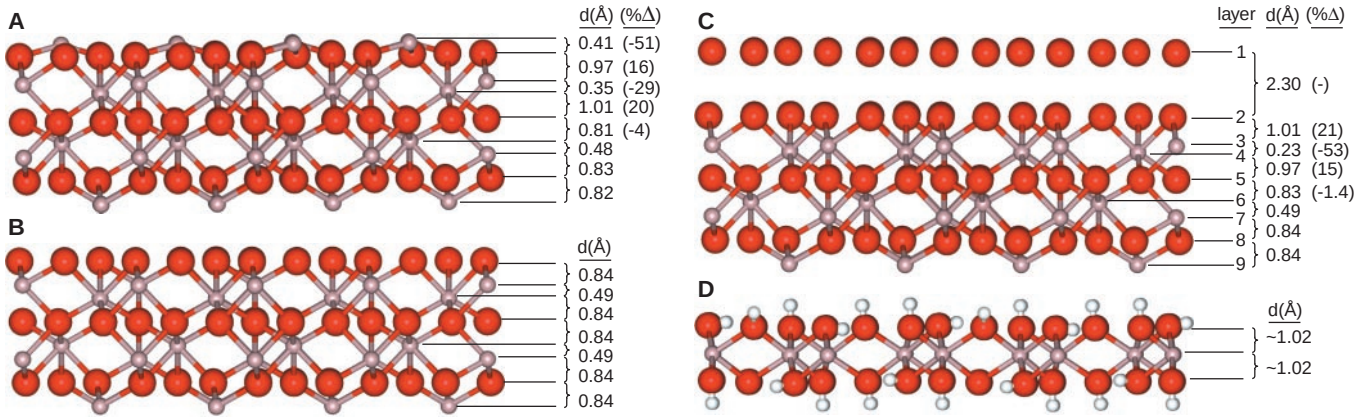

Fig. 2. (**A** to **C**) Atomic layering sequence and layer spacings (*d*) along the [0001] direction is shown for various terminations of the α-Al_2O_3 surface. Red, silver, and gray spheres indicate O, Al, and H atoms, respectively. (A) Single Al-terminated surface model from Guenard *et al*. (*17, 29*). (B) Ideal (unrelaxed) oxygen-terminated surface. (C) Best-fit relaxed surface model for the oxygen-terminated surface from this work, including the oxygen overlayer (layer 1). (**D**) Side view of a layer sequence from the gibbsite structure. In (A) and (C), %Δ is the percent change in layer spacing from the ideal termination (B).

sults of studies of water sorption versus relative humidity on α-Al_2O_3 powder, which show that, under typical atmospheric conditions (298 K and 50 to 60% relative humidity), about three monolayers of water are adsorbed on alumina surfaces (*26*). Inclusion of this oxygen overlayer (Fig. 1A, solid lines) resulted in a significantly improved fit to the (00L) rod and an overall reduction in χ^2 to 1.37, which indicates that layer order exists for approximately one of the adsorbed layers (*27*).

The coordinates of the best-fit model and the ideal oxygen-terminated surface are compared in Table 1 (*28*). The predominant structural change relative to the bulk termination is the large relaxation of layer 3 and 4 Al atoms toward a common plane, resulting in a 53% contraction of the layer spacing. The changes in the positions of the layer 2 and layer 5 oxygen atoms are negligible within the estimated error ranges. However, contraction of the Al-layer spacing leads to significant expansion of the layer spacing between layers 2 and 3 (21%) and between layers 4 and 5 (15%) (Fig. 2C).

In addition to the large surface relaxation observed, the fitted values for layer 1 oxygens result in a *d* spacing of about 2.3 ± 0.4 Å (Fig. 2C), which is reasonable for hydrogen bonding of overlayer water to surface hydroxyl groups. However, our XPS measurements show a carbon concentration of about 21 atoms/nm^2, which accounts for less than 50% of the overlayer composition compared with the estimated quantity of adsorbed water. Given the carbon concentration and the similarity in scattering power of C and O, we were unable to identify the location of the C in the overlayer. Therefore, we assumed that this laterally disordered layer 2.3 Å above the surface could be a mixture of hydrogen-bonded water and adventitious carbon. Even though the overall fit is improved by including this layer, its presence in the model has an insignificant effect on the fitted atomic positions of the relaxed surface.

We conclude that, under the conditions of our study, the α-Al_2O_3 (0001) surface is oxygen terminated with a large relaxation of the layer 3 and 4 Al and a partly ordered, physisorbed water or mixed water/hydrocarbon overlayer (Fig. 2C). This result differs markedly from previous studies of the ultrahigh vacuum (UHV)-prepared clean α-Al_2O_3 (0001) surface, which found that the best model was the single Al-terminated surface

Table 1. Fractional coordinates (a = 4.757 Å, c = 12.988 Å) of atoms in the surface model for perfect oxygen termination (bulk termination) and best-fit relaxed surface. Estimated errors from the least-squares fit at the 96% confidence level are given in parentheses. Values without reported errors were held fixed in the fits. The Δz values are the change in layer z position with respect to the perfect termination. Bond valence sums (Σs) were calculated according to the method of Brown and Altermatt (*33*).

Layer		Bulk termination			Relaxed surface						
		x	Y	z	x	Y	z	Δz(Å)	B_{iso}(Å^2)	Occupancies	Σ*s* (v.u.)
1	O	—	—	—	0.01 (1)	0.65 (1)	1.59 (2)	—	32 (8)	2.0 (4)	—
	O	—	—	—	0.35 (1)	0.36 (1)	1.59 (2)	—	32 (8)	2.0 (4)	—
	O	—	—	—	0.64 (1)	0.99 (1)	1.59 (2)	—	32 (8)	2.0 (4)	—
2	O	0.027	0.667	1.417	0.03 (1)	0.67 (1)	1.419 (3)	0.03 (4)	5 (2)	1.0	0.98 (4)
	O	0.333	0.360	1.417	0.33 (1)	0.36 (1)	1.419 (3)	0.03 (4)	5 (2)	1.0	0.98 (4)
	O	0.640	0.973	1.417	0.64 (1)	0.97 (1)	1.419 (3)	0.03 (4)	5 (2)	1.0	0.98 (4)
3	Al	0.000	0.000	1.352	0.000	0.000	1.341 (1)	−0.14 (1)	0.32	0.89 (5)	3.0 (1)
4	Al	0.333	0.667	1.314	0.333	0.667	1.323 (1)	0.11 (2)	0.32	0.96 (4)	3.0 (2)
5	O	0.306	0.000	1.250	0.306	0.000	1.249 (2)	−0.01 (2)	0.33	1.0	2.04 (4)
	O	0.000	0.306	1.250	0.000	0.306	1.249 (2)	−0.01 (2)	0.33	1.0	2.04 (2)
	O	0.694	0.694	1.250	0.694	0.694	1.249 (2)	−0.01 (2)	0.33	1.0	2.04 (2)
6	Al	0.667	0.333	1.186	0.667	0.333	1.186	0.00	0.32	1.0	3.02 (5)
7	Al	0.000	0.000	1.148	0.000	0.000	1.148	0.00	0.32	1.0	3.03 (6)
8	O	0.360	0.333	1.083	0.360	0.333	1.083	0.00	0.33	1.0	2.00
	O	0.667	0.027	1.083	0.667	0.027	1.083	0.00	0.33	1.0	2.00
	O	0.973	0.640	1.083	0.973	0.640	1.083	0.00	0.33	1.0	2.00
9	Al	0.333	0.667	1.019	0.333	0.667	1.019	0.00	0.32	1.0	3.00

(Figs. 1B and 2A) or mixed Al/O-terminated surface (*29*). The single Al-terminated surface is thought to be most stable under UHV conditions because it results in a net zero surface dipole (*30*). Several theoretical studies (*8–14*) also conclude that this is the stable termination and predict Al relaxations of magnitude similar to those measured. However, it has also been shown experimentally (*5–7, 31, 32*) and theoretically (*8–10*) that the clean α-Al_2O_3 (0001) surface readily reacts with water.

The stability of the relaxed surface relative to the UHV clean surface was examined by bond valence analysis (Table 1) using the empirical formulation of the bond-length bond-strength relationship of Brown and Altermatt (*33*). Based on the Pauling electrostatic bond valence principle, the sum of the bond valence s [expressed in valence units (v.u.)] from each nearest neighbor should equal the magnitude of the valence of the given atom (*34*). The bond valence sums for the layer 3 to layer 7 atoms in our best-fit model satisfy the electrostatic valence principle (Table 1). However, the layer 2 oxygen has a bond valence sum of about 1.0, which is expected because it has two dangling bonds. Based on the work of Bargar *et al.* (*35*), the binding of a single proton in a hydroxyl group (OH) contributes $0.67 < s_{OH} < 0.79$ v.u. to the oxygen, whereas a hydrogen bond (O $\cdots$ H) contributes $0.18 < s_{O\cdots H} < 0.31$ v.u. Therefore, addition of two directly bound protons leads to oversaturation of the oxygen, whereas inclusion of a single proton and a hydrogen bond satisfies the surface oxygen bond valence sum. Accordingly, undersaturation of the bare oxygen atoms in layer 2 can be accounted for by direct binding of protons and additional hydrogen bonding, leading to its interpretation as a surface hydroxyl layer. In comparison, the bond valence sum for the terminal Al in the Al-terminated UHV clean surface (Fig. 2A) is about 2.2 v.u. Therefore, because of undersaturation of the surface Al, the Al-terminated surface is expected to be highly reactive when it is in contact with water, whereas the OH-terminated surface is expected to be stable if sufficient hydrogen bonding contributions are made by adsorbed water or by in-plane hydrogen bonding.

Because of the weak x-ray scattering power of protons, the presence of surface hydroxyl groups can only be inferred from the above analysis. In support of this inference, however, is the fact that the relaxed surface (Fig. 2C, layers 2 to 5) resembles an intermediate between the structure of the gibbsite [γ-$Al(OH)_3$] or bayerite [α-$Al(OH)_3$] basal plane (Fig. 2D) and the ideal α-Al_2O_3 basal plane (Fig. 2B). In both the gibbsite and bayerite structures, the Al ions reside approximately in a single plane and have distorted octahedral coordination with a double layer of closest-packed OH ions (*36*). Furthermore, gibbsite and bayerite are expected to be more stable than α-Al_2O_3 under high partial pressures of water (*36*). The large 53% contraction we observe for the staggered double Al layer (Fig. 2C, layers 3 and 4) can be interpreted as the structure moving toward a more stable gibbsite/bayerite-like atomic arrangement, driven by the presence of the layer 2 hydroxyls (*37*).

The presence of hydroxyl groups on the surface with hydrogen-bonding contributions also is supported by recent theoretical calculations of the interaction of water with α-Al_2O_3 (0001) surfaces. These studies suggest that, under sufficiently high water loadings, the surface Al atoms on the single Al-terminated surface convert to terminal $AlO_3(OH)_3$ species, which should be highly labile, and their removal or diffusion results in a OH-terminated surface (*8, 10*). The simulations of Hass *et al*. (*8*) on the OH-terminated surface suggest that extensive hydrogen bonding occurs in-plane among the surface hydroxyls and that the hydrogen bonding is dynamic, with an average of one of three hydroxyls lying in the surface plane. The dynamic nature of the hydrogen bonding is likely reflected in the Debye-Waller factors found in our least-squares refinement, which gives a root-mean-square (rms) displacement of about 0.25 Å for layer 2 oxygens. Furthermore, based on the findings of Hass *et al.* (*8*), the hydrogen bonding required to complete the valence saturation of the layer 2 oxygen in our best-fit model appears to be obtainable from in-plane hydrogen-bonding contributions, although additional hydrogen bonding from overlayer water is also likely.

Often it is assumed that the reaction of water with metal oxide surfaces will complete the first coordination shell of coordinatively unsaturated metal ions and that this leads to a simple (unrelaxed) oxygen-terminated surface. For the hydrated α-Al_2O_3 (0001) surface, we find that the first point is true; however, surface hydroxylation in this case leads to significant surface relaxation. We expect that the coordinatively saturated, hydroxyl-terminated alumina surface will be much less reactive toward water and that conversion of the outermost surface to a gibbsite/bayerite-like atomic arrangement essentially passivates the surface. These suggestions are consistent with the findings of past attenuated total reflectance Fourier transform infrared and photoemission studies of the hydration of α-Al_2O_3 (*37*), which show that only the surface region of alumina is hydroxylated. On the basis of our structural model, reactivity of the hydrated alumina surface should be similar to that of the gibbsite and bayerite basal planes, which are dominated by $Al_2(OH)$ surface groups. These findings have direct implications for recent site-specific models of metal-ion adsorption at the alumina (0001)–water interface derived from grazing-incidence x-ray adsorption fine structure (XAFS) spectroscopy results for Pb(II) (*35*), Co(II) (*38*), and Cu(II) (*39*) chemisorbed on alumina. Derivation of these adsorption models depends on measured distances between the adsorbed metal ion and Al second-neighbor cations in the substrate and, therefore, on assumptions about the atomic arrangement of the outer layers of the alumina (0001) surface. In a recent XAFS study of Cu(II) sorption at the alumina (0001)–water interface (*39*), for example, it was found that the most plausible model required relaxation of the alumina surface structure similar to that found in this study.

The results of this study confirm that the reactivity of the UHV clean surface should differ markedly from an alumina surface prepared in the presence of water. For example, Kelber *et al*. (*40*) observed that Cu growth on a partially hydroxylated α-Al_2O_3 (0001) surface is dominated by two-dimensional island formation, whereas Cu growth on dehydroxylated surfaces is likely dominated by three-dimensional island formation. The surface Al sites in the Al-terminated model are strong Lewis acid sites, whereas the OH groups in the OH-terminated surface are Lewis bases. After hydroxylation of the α-Al_2O_3 (0001) surface, all surface sites become Lewis bases with lowered reactivity to water but enhanced overall reactivity toward metals.

References and Notes

1. G. E. Brown Jr. *et al*., *Chem. Rev.* **99**, 77 (1999).
2. H. Knozinger and P. Ratnasamy, *Catal. Rev. Sci. Eng.* **17**, 31 (1978).
3. P. A. Thiel and T. E. Madey, *Surf. Sci. Rep.* **7**, 211 (1987).
4. B. C. Gates, *Catalytic Chemistry* (Wiley, New York, 1992).
5. P. Liu, T. Kendelewicz, G. E. Brown Jr., E. J. Nelson, S. A. Chambers, *Surf. Sci.* **417**, 53 (1998).
6. J. W. Elam, C. E. Nelson, M. A. Cameron, M. A. Tolbert, S. M. George, *J. Phys. Chem. B* **102**, 7008 (1998).
7. C. E. Nelson, J. W. Elam, M. A. Cameron, M. A. Tolbert, S. M. George, *Surf. Sci.* **416**, 341 (1998).
8. K. C. Hass, W. F. Schneider, A. Curioni, W. Andreoni, *Science* **282**, 265 (1998).
9. J. M. Wittbrodt, W. L. Hase, H. B. Schlegel, *J. Phys. Chem. B* **102**, 6539 (1998).
10. R. Di Felice and J. E. Northrop, *Phys. Rev. B* **60**, R16 287 (1999).
11. C. Verdozzi, D. R. Jennison, P. A. Schultz, M. P. Sears, *Phys. Rev. Lett.* **82**, 799 (1999).
12. V. E. Puchin *et al*., *Surf. Sci.* **370**, 190 (1997);
13. T. J. Godin and J. P. LaFemina, *Phys. Rev. B* **49**, 7691 (1994).
14. I. Manassidis, A. De Vita, M. J. Gillan, *Surf. Sci.* **285**, L517 (1993).
15. J. Toofan and P. R. Watson, *Surf. Sci.* **401**, 162 (1998).

16. J. Ahn and J. W. Rabalais, *Surf. Sci.* **388**, 121 (1997).
17. P. Guenard, G. Renaud, A. Barbier, M. Gautier-Soyer, *Surf. Rev. Lett.* **5**, 321 (1997).
18. T. Hiemstra, H. Yong, W. H. Van Riemsdijk, *Langmuir* **15**, 5942 (1999).
19. D. A. Sverjensky and N. Sahai, *Geochim. Cosmochim. Acta* **60**, 3773 (1996).
20. CTR diffraction is done by measuring diffuse scattering between Bragg points as a function of perpendicular momentum transfer into the substrate. This diffuse CTR scattering aligns normal to the surface and arises from breaking bulk translation symmetry due to the presence of an interface or surface. Surface relaxations and reconstructions and the presence of overlayer atoms modulate the signal along these rods of scattering. For an introduction to the technique see I. K. Robinson and D. J. Tweet, *Rep. Prog. Phys.* **55**, 599 (1992); G. Renaud, *Surf. Sci. Rep.* **32**, 1 (1998); P. Fenter *et al.*, *Geochim. Cosmochim. Acta* 64, 1221 (2000).
21. The crystal wafer obtained from Union Carbide Crystal Products (Washougal, WA) was 0.5 mm thick and 50 mm in diameter, with a rms roughness of about 1 Å, based on x-ray reflectivity measurements, and a miscut of $<0.3°$, based on orientation measurements during the CTR work. The wafer was prepared with a mild acid etch (10 mM HNO_3) followed by multiple rinses with MilliQ water and heating to 350°C in air. After cooling to room temperature, it was immediately subjected to an extensive wash with MilliQ water and blown dry with an argon jet. Similarly prepared wafers have been studied by our group using photoemission and atomic force microscope, as reported in (*5*).
22. In previous work (*5*–*9*), the hydration reaction was found to be dissociative, leading to surface hydroxyl groups.
23. The structure factor is determined by taking the square root of the background-subtracted integrated intensity corrected for active area, polarization, step size, and Lorentz factor [I. K. Robinson, in *Handbook on Synchroton Radiation*, vol. 3, G. Brown and D. E. Moncton, Eds. (Elsevier, Amsterdam, 1991), pp. 221–266].
24. The structure of α-Al_2O_3 (space group $R\bar{3}c$) consists of a distorted hexagonal close-packed layer sequence of oxygens, with aluminum occupying two-thirds of the octahedral holes. The oxygen stacking sequence runs along the *c* axis, and a unit cell consists of six oxygen layers, giving six formula units per unit cell. The Al atoms are staggered along the *c* direction about a plane centered between the oxygen layers, and the oxygen atoms are slightly displaced in-plane from their ideal positions. The staggered positions of the Al atoms lead to two sets of Al-O bond lengths. The Al that is displaced in the positive direction along the *c* axis has three short Al-O bonds (1.86 Å) to the oxygen layer above and three long Al-O bonds (1.97 Å) to the oxygen layer below. The reverse is the case for the Al that is displaced in the negative direction along the *c* axis. The cell parameters used in this work ($a = 4.757$ Å, $c = 12.988$ Å) are from [A. Kirfel and K. Eichhorn, *Acta Crystallogr. A* **46**, 271 (1990)], with bulk isotropic Debye-Waller factors from [N. Ishizawa, T. Miyata, I. Minato, F. Marumo, S. Iwai, *Acta Crystallogr. B* **36**, 228 (1980)].
25. For each of the three chemical terminations, there are six crystallographically distinct terminations depending on where the unit cell is cut. Because they are chemically equivalent, the six terminations must be equally probable, and therefore our model consisted of equal weighting of these terminations, with the same fit parameters (displacements, Debye-Waller factors, and occupancies) used for each.
26. B.-D. Yan, S. L. Meilink, G. W. Warren, P. Wynblatt, *IEEE Trans. Components Hybrids Manufact. Technol.* **CHMT-10**, 247 (1987).
27. The (00L) rod is sensitive only to ordering in the direction perpendicular to the surface and is unaffected by the degree of lateral ordering. The dominant free parameter in the overlayer model is the *z* position of the layer. The Debye-Waller factor acts as a measure of layer disorder even though the actual structure is likely to be more complex. A more accurate description of the layer involves a continuous electron density distribution normal to the surface; however, extensive specular reflectivity data are required to uniquely determine such a distribution.
28. Seven independent displacement parameters, four Debye-Waller factors, and four layer occupancies were used in the least-squares fitting procedure. Only the parameters for the top five layers were allowed to vary in the final fit. Varying additional parameters for deeper layers did not significantly improve the χ^2 value; therefore, they were held at their bulk positions in the final fit. The α-Al_2O_3 (0001) surface has p3 symmetry, with Al atoms positioned at the centers of the threefold axis and the oxygens arranged about the threefold axis. To maintain symmetry in our surface model, we displaced the Al atoms only along the *z* direction and we constrained the oxygen atoms to maintain trigonal symmetry.
29. There exists some debate (*15*–*17*) about the termination as well as the layer spacing for the clean UHV surface. Guenard *et al.* (*17*) find (Fig. 2A) an Al-terminated surface with a 51% contraction for the first layer, whereas Ahn and Rabalais (*16*) find a 63% contraction. Toofan and Watson (*15*) find a mixed Al/O termination with expansion of the top layer. Surface preparation variation resulting in, for example, residual OH could account for these differences.
30. M. Gautier *et al.*, *J. Am. Ceram. Soc.* **77**, 323 (1994).
31. V. Coustet and J. Jupille, *Surf. Sci.* **307-309**, 1161 (1994).
32. J. G. Chen, J. E. Crowell, J. T. Yates, *J. Chem. Phys.* **84**, 5906 (1986).
33. I. D. Brown and D. Altermatt, *Acta Crystallogr. B* **41**, 244 (1985).
34. L. Pauling, *The Nature of the Chemical Bond* (Cornell University Press, Ithaca, NY, ed. 3, 1960), pp. 547–559.
35. J. R. Bargar, S. N. Towle, G. E. Brown Jr., G. A. Parks, *J. Colloid Interface Sci.* **185**, 473 (1997).
36. K. Wefers and C. Misra, *Oxides and Hydroxides of Aluminum*, *Alcoa Technical Paper No. 19, Revised* (Alcoa Laboratories, Alcoa Center, PA, 1987).
37. Differences in stability were used by Liu *et al.* (*5*) to predict the threshold pressure for hydroxylation of the α-Al_2O_3 (0001) surface to be 2.8 torr and 6.3 torr based on gibbsite and bayerite free energies, respectively. This result agrees well with the measured threshold pressure of about 1 torr for hydroxylation of the α-Al_2O_3 (0001) surface, as determined by O 1s photoemission spectroscopy (*5*). It has also been observed that Al hydroxides (gibbsite and bayerite) are formed on water-immersed α-Al_2O_3 [D. H. Lee and R. A. Condrate Sr., *Mater. Lett.* **23**, 241 (1995)] and γ-Al_2O_3 [C. Dyer, P. J. Hendra, W. Forsling, M. Ranheimer, *Spectrochim. Acta* **49A**, 691 (1993); E. Laiti, P. Persson, L-O. Öhman, *Langmuir* **14**, 825 (1998)] powder surfaces.
38. S. N. Towle, J. R. Bargar, G. E. Brown Jr., G. A. Parks, *J. Colloid Interface Sci.* **217**, 312 (1999).
39. J. P. Fitts, T. P. Trainor, D. Grolimund, G. E. Brown Jr., G. A. Parks, unpublished data.
40. J. A. Kelber, C. Niu, K. Shepherd, D. R. Jennison, A. Bogicevic, *Surf. Sci.* **446**, 76 (2000).
41. Supported by Department of Energy (DOE) grant DE-FG03-93ER14347-A007 (Stanford University), DOE grant DE-FGO2-94ER14466, National Science Foundation grant EAR-9906456, and the W. M. Keck foundation (GeoSoilEnviroCARS, University of Chicago). Use of the Advanced Photon Source was supported by the DOE, Basic Energy Sciences, Office of Energy Research, under contract W-31-109-ENG-38. We thank J. Fitts, D. Grolimund, F. Sopron, and N. Lazarz for their assistance with the measurements and J. V. Smith for constructive comments on the manuscript.

21 December 1999; accepted 22 March 2000

Rapid Flooding of the Sunda Shelf: A Late-Glacial Sea-Level Record

Till Hanebuth,* Karl Stattegger, Pieter M. Grootes

The increase in sea level from the last glacial maximum has been derived from a siliciclastic system on the tectonically stable Sunda Shelf in Southeast Asia. The time from 21 to 14 thousand calendar years before the present has been poorly covered in other records. The record generally confirms sea-level reconstructions from coral reefs. The rise of sea level during meltwater pulse 1A was as much as 16 meters within 300 years (14.6 to 14.3 thousand years ago).

Sea-level curves of the last deglaciation have been constructed from coral reefs by means of U/Th or radiocarbon dating of corals [e.g., Barbados (*1, 2*), Tahiti (*3*, *4*), New Guinea (*5, 6*)]. The Barbados record contains only a few clustered data points between larger intervals without data for the early phase of the late-glacial sea-level rise; the Tahiti record starts at 13.8 thousand years ago (ka) (all ages are in calendar kiloyears before present) (*7*) above a late Pleistocene reef unit; and the New Guinea record starts at 13.1 ka and is situated in an area with strong tectonic uplift. There is a prominent hiatus in most records corresponding to the meltwater pulse (MWP) 1A around 14 ka (*2*). Catastrophic sea-level rise for that time is interpreted in the Caribbean-Atlantic region from an abrupt deepening of the coral assemblages (*8*). From these and other records, two alternative models of the eustatic late- to postglacial sea-level rise have been proposed (*9*): (i) a continuous model in which sea level rose steadily with varying transgression rates and (ii) an episodic model in which sea level rose in steps with several pauses or even erosion in between.

Here we present a record of the late-glacial transgression on the Sunda Shelf, the largest shelf area outside the polar regions, covering an area of 1.8×10^6 km^2 between the Indonesian archipelago and Vietnam. During the last glacial

Institute of Geosciences, University of Kiel, Olshausenstrasse 40, 24 118 Kiel, Germany.

*To whom correspondence should be addressed. E-mail: th@gpi.uni-kiel.de